

38 **Abstract**

39 Swarmer cells of the gram-negative pathogenic bacteria *Proteus mirabilis* and *Vibrio*
40 *parahaemolyticus* become long (>10-100 μm) and multinucleate during their growth and
41 motility on polymer surfaces. We demonstrate increasing cell length is accompanied by
42 a large increase in flexibility. Using a microfluidic assay to measure single-cell
43 mechanics, we identified large differences in swarmer cell stiffness of (bending rigidity
44 of *P. mirabilis*, $9.6 \times 10^{-22} \text{ N m}^2$; *V. parahaemolyticus*, $9.7 \times 10^{-23} \text{ N m}^2$) compared to
45 vegetative cells ($1.4 \times 10^{-20} \text{ N m}^2$ and $3.2 \times 10^{-22} \text{ N m}^2$, respectively). The reduction in
46 bending rigidity (~3-15 fold) was accompanied by a decrease in the average
47 polysaccharide strand length of the peptidoglycan layer of the cell wall from 28-30 to
48 19-22 disaccharides. Atomic force microscopy revealed a reduction in *P. mirabilis*
49 peptidoglycan thickness from 1.5 nm (vegetative) to 1.0 nm (swarmer) and electron
50 cryotomography indicated changes in swarmer cell wall morphology. *P. mirabilis* and *V.*
51 *parahaemolyticus* swarmer cells became increasingly sensitive to osmotic pressure and
52 susceptible to cell wall-modifying antibiotics (compared to vegetative cells)—they were
53 ~30% more likely to die after 3 h of treatment with minimum inhibitory concentrations
54 of the β -lactams cephalexin and penicillin G. Long, flexible swarmer cells enables these
55 pathogenic bacteria to form multicellular structures and promotes community motility.
56 The adaptive cost of swarming is offset by a fitness cost in which cells are more
57 susceptible to physical and chemical changes in their environment, thereby suggesting

58 the development of new chemotherapies for bacteria that leverage swarming for
59 survival.

60

61 **Significance Statement**

62 *Proteus mirabilis* and *Vibrio parahaemolyticus* are bacteria that infect humans. To adapt to
63 environmental changes, these bacteria alter their cell morphology and move collectively
64 to access new sources of nutrients in a process referred to as ‘swarming’. We found that
65 a change in the composition and thickness of the peptidoglycan layer of the cell wall
66 makes swarmer cells of *P. mirabilis* and *V. parahaemolyticus* more flexible (i.e., reduced
67 cell stiffness) and increases their sensitivity to osmotic pressure and cell-wall targeting
68 antibiotics (e.g., β -lactams). These results highlight the importance of assessing the
69 extracellular environment in determining antibiotic doses and the use of β -lactams
70 antibiotics for treating infections caused by swarmer cells of *P. mirabilis* and *V.*
71 *parahaemolyticus*.

72 “\body”

73

74

75

76

77

78 **Introduction**

79 Bacteria have evolved a variety of mechanisms to adapt to their physical environment.
80 For example, in response to fluctuating environmental conditions, changes in
81 biochemistry and gene regulation can alter bacterial shape and increase cell fitness. Cell
82 filamentation is a commonly observed change in bacterial cell shape (1, 2) and has been
83 described as a mechanism that enables bacteria to evade predation by the innate
84 immune system during host infections (1).

85 In close proximity to surfaces, many bacteria alter their morphology and leverage
86 cell-cell physical contact to move collectively to access new sources of nutrients and
87 growth factors (3, 4). Referred to as ‘swarming’, this process is common among motile
88 bacteria, has been connected to bacterial pathogenesis and infections, and is an example
89 of adaptive behavior (3, 4). Swarmer cells of *Salmonella enterica*, *Pseudomonas aeruginosa*,
90 *Serratia marcescens*, and *Bacillus subtilis* have reduced susceptibility – compared to
91 vegetative cells – to a variety of antibiotics that target protein translation, DNA
92 transcription, and the bacterial cell membrane and cell wall (5-8). The specific
93 biochemical and biophysical mechanisms underlying these observations are unknown.

94 Here, we describe physical changes in swarmer cells of the gram-negative
95 pathogenic bacteria *Proteus mirabilis* and *Vibrio parahaemolyticus* that increase their
96 susceptibility to cell wall-targeting clinical antibiotics. We found that large changes in
97 the length of *P. mirabilis* and *V. parahaemolyticus* swarmer cells are accompanied by an

98 increase in flexibility (i.e., a reduction in cell stiffness) that enables long cells to pack
99 together tightly and form cell-cell interactions; these interactions have been
100 demonstrated previously to promote surface motility (9). Using biophysical,
101 biochemical, and structural techniques, we quantified changes in the structure and
102 composition of the *P. mirabilis* and *V. parahaemolyticus* cell wall in swarmer and
103 vegetative cells and characterized their susceptibility to osmotic changes and cell wall-
104 modifying antibiotics. Our results indicate that morphological changes that enable these
105 bacteria to adapt to new physical environments come at a significant fitness cost: cells
106 become more susceptible to changes in their chemical environment. These results
107 predict cell wall-modifying antibiotics should deter infections of *P. mirabilis* and *V.*
108 *parahaemolyticus* in which swarming is implicated (e.g., in urinary tract infections).

109

110 **Results**

111 **The bending rigidity of *P. mirabilis* and *V. parahaemolyticus* cells decreases during**
112 **swarming.** During surface motility, *P. mirabilis* and *V. parahaemolyticus* cells grow into
113 swarmers that are characteristically long (10-100 μm) and present a high surface density
114 of flagella that enables them to translate through viscous environments (3, 10). We
115 found that these swarmer cells display an unusual phenotype that is rarely observed
116 among gram-negative bacteria: cells become remarkably flexible and their shape is
117 dynamically altered by adjacent cell motion and collisions (Fig. 1). The ability of *P.*

118 *mirabilis* swarmer cells to form cell-cell contacts plays a role in their cooperative motility
119 (10), leading us to hypothesize that increasing flexibility enables these long cells to
120 optimize packing into multicellular structures that move cooperatively across surfaces.
121 Bacterial cell mechanics is generally attributed to the peptidoglycan (PG) layer of the
122 cell wall, which has a thickness of ~3-50 nm and surrounds the cytoplasmic membrane
123 (11). Very little is known about mechanical regulation in bacteria (12-17) and we are
124 unaware of studies connecting swarming to changes in cell mechanics. We quantified
125 changes in swarmer-cell stiffness using cell-bending assays in a reloadable,
126 poly(dimethylsiloxane) microfluidic system (Fig. 2 and S1) that is related to a method
127 developed previously (18). In bending assays, we applied a shear fluid force to multiple
128 filamentous cells, resulting in horizontal deflection of their cell tips (Fig. 2); fitting the
129 deflection data to a mechanical model provided us with a value of the (flexural)
130 bending rigidity of cells (Fig. S2). Introducing a reloadable mechanism enabled us to
131 perform rapid bending measurements of *P. mirabilis* and *V. parahaemolyticus* swarmer
132 cells after isolating them from swarm plates. As a point of comparison, we filamented
133 vegetative cells of *P. mirabilis* and *V. parahaemolyticus* using aztreonam—an inhibitor of
134 the division specific transpeptidase PBP3—to match the length of swarmer cells and
135 compared their bending rigidity values to swarmer cells. As a control, we measured the
136 bending rigidity of cells of *Escherichia coli* strain MG1655 that we filamented using
137 aztreonam, and determined the value to be 9.7×10^{-23} N m² (Fig. 3); using a value for the

138 thickness of the PG of 4-nm (19) yields a Young's modulus of 26 MPa, which is close to
139 values that have been reported previously (12, 18).

140 We used bending rigidity as a parameter to quantify *P. mirabilis* and *V.*
141 *parahaemolyticus* cell stiffness rather than Young's modulus, as the latter metric of the
142 mechanical properties of materials is dependent on cell-wall thickness, which we
143 hypothesized may change during swarming (described below). We found a substantial
144 decrease in the bending rigidity of swarmer cells of both *P. mirabilis* (~15-fold) and *V.*
145 *parahaemolyticus* (3-fold) compared to their vegetative cell counterparts (Fig. 3), which is
146 consistent with our observations of the shape and behavior of these cells during
147 swarming on surfaces. *V. parahaemolyticus* vegetative cells were remarkably flexible:
148 ~134-fold more so than *E. coli* cells and ~3-fold more than *P. mirabilis* swarmer cells (Fig.
149 3).

150 To confirm that using aztreonam to inhibit PBP3 and produce filamentous cells
151 did not change the cross-linking density of PG at the division plane and alter cell
152 mechanics, we compared bending rigidity values of cells treated with aztreonam and
153 cells filamented by overexpressing SulA, a protein that prevents polymerization of the
154 division protein FtsZ and blocks cell division. Both mechanisms of filamenting *E. coli*
155 cells produced similar bending rigidity values: 4.0×10^{-20} N m² (SulA) and 4.1×10^{-20} N
156 m² (aztreonam) (Fig. S4A). To account for the high surface density of flagella on
157 swarmer cells, which may contribute to cell drag in fluid flow and bias measurements,

158 we performed bending rigidity measurements (Fig. S4B) on two K-12-derived strains of
159 *E. coli* with substantially different flagella densities (Fig. S4C) and observed no
160 appreciable change in values (bending rigidity of 4.0×10^{-20} N m² at high flagella density
161 and 4.1×10^{-23} N m² at low flagella density; Fig. S4B).

162 Overexpressing FlhDC—the heterohexameric activator that is important for
163 swarming—in vegetative cells growing in liquid produces a phenotype that replicates
164 many of the characteristics of swarmer cells, including increased cell length and flagella
165 density (20). The relationship between FlhDC and cell mechanics has not yet been
166 reported. To test whether FlhDC is connected to changes in swarmer cell stiffness, we
167 overexpressed the protein from the plasmid-encoded genes *pflhDC* in filamentous cells
168 of *P. mirabilis* and measured their bending rigidity. We detected a ~1.5-fold difference in
169 bending rigidity between wildtype (1.4×10^{-20} N m²) and *pflhDC*-containing *P. mirabilis*
170 vegetative cells (9.2×10^{-21} N m²), and no difference compared to *pflhDC*-containing *P.*
171 *mirabilis* swarmer cells (Fig. 3). These results indicate that FlhDC overexpression during
172 swarming contributes a small amount to the mechanical phenotype of swarming cells,
173 however the majority of the mechanical changes we observe arises from PG alterations
174 through another regulatory pathway.

175

176 **Changes in PG composition of *P. mirabilis* and *V. parahaemolyticus* swarmer cells.**

177 PG consists of the disaccharide building block β -(1,4)-N-acetylmuramic acid/N-acetyl-

178 glucosamine (MurNAc-GlcNAc) in which a pentapeptide is attached to each 3'-OH
179 group on MurNAc. Cross-linking between adjacent pentapeptides creates a mesh-like
180 polymeric layer, and altering its structure and composition affects cell-mechanical
181 properties (14, 15). To determine whether the PG composition of *P. mirabilis* and *V.*
182 *parahaemolyticus* cells changes during swarming, we isolated PG sacculi from vegetative
183 and swarmer cells and used ultra performance liquid chromatography-mass
184 spectrometry (UPLC-MS) to quantify its chemical composition (Fig. S5). As the PG
185 composition of *V. parahaemolyticus* has not yet been reported, we characterized its
186 muropeptide stem peptide using UPLC-MS/MS (Fig. S6 and Table S1). Similar to *E. coli*
187 (21) and *P. mirabilis* (22), *V. parahaemolyticus* has a PG structure that is conserved across
188 other gram-negative bacteria, in which the peptide stem consists of L-Ala-D-Glu-*meso*-
189 diaminopimelic acid (*meso*-DAP)-D-Ala-D-Ala (Fig. S6).

190 Compared to vegetative cells, *P. mirabilis* swarmer cells contained fewer
191 monomers (MurNAc-GlcNAc), more dimers, and more anhydrous-containing
192 saccharides, which are found at the terminating end of glycan polymers (Fig. 4A) (11).
193 We detected no differences in the relative abundance of trimers between swarmer and
194 vegetative cells of *P. mirabilis* (Fig. 4A). The increase in anhydrous-containing
195 saccharides that we observed in *P. mirabilis* swarmer cells was correlated with a
196 decrease in polysaccharide length (Fig. 4B; the values plotted reflect the number of
197 MurNAc-GlcNAc dimers). A similar increase in anhydrous-containing saccharides and

198 decreased length of polysaccharides occurred in *V. parahaemolyticus* swarmer cells (Fig.
199 4A, B). We found no change in cross-linking density between vegetative and swarmer
200 cells of either *P. mirabilis* or *V. parahaemolyticus* (Fig. 4C).

201

202 **Swarmer cells have a reduced PG thickness and display membrane defects.** Changes
203 in the thickness of the PG layer and structure of the cell envelope may also explain the
204 observed decrease in swarmer cell stiffness. To identify changes in PG thickness of
205 swarmer cells, we isolated the intact layer of PG (i.e., sacculi) from *P. mirabilis*
206 vegetative and swarmer cells and measured the thickness of dried sacculi using
207 tapping-mode atomic force microscopy (AFM) (Fig. 5A). Differences in the nanoscopic
208 appearance of the sacculi of different cells were not observed by AFM (Fig. S7). The
209 thickness of isolated, dry *P. mirabilis* swarmer cell sacculi (1.0 ± 0.2 nm) was reduced
210 ~1.5-fold compared to vegetative cells (1.5 ± 0.2 nm) (Fig. 5A). *V. parahaemolyticus*
211 swarmer cells (0.6 ± 0.1 nm) exhibited a similar ~1.2-fold decrease in thickness
212 compared to vegetative cells (0.8 ± 0.2 nm). Earlier AFM measurements of isolated
213 sacculi indicated that dehydration reduced the thickness of *Escherichia coli* PG by ~2x,
214 which we used to estimate the dimensions of hydrated PG from *P. mirabilis* (3.1 and 2.1
215 nm for vegetative and swarmer cells, respectively) and *V. parahaemolyticus* (1.7 and 1.4
216 nm, respectively) (23). A comparison of PG thickness and cell bending rigidity

217 suggested that the relationship between these data is approximately exponential
218 ($R^2=0.9874$) (Fig. 5B).

219 A caveat with conversions between dried and hydrated values is that they will
220 be most accurate for PG that best mimics the structure and composition (e.g.,
221 crosslinking and polysaccharide composition) of the reference material: *E. coli* PG.
222 Alterations in the polysaccharide length of PG from *P. mirabilis* and *V. parahaemolyticus*
223 may be more elastic and stretch out during drying, thereby appearing to have a
224 thickness that is reduced compared to *E. coli* PG. Our control measurements on isolated,
225 dry *E. coli* sacculi yielded a thickness of 2.0 nm, which varies from the value of 3.0 nm
226 published by Yao et al. using the same technique (23). A difference of ~30% between
227 these *E. coli* measurements may arise for several reasons, including: variations in
228 physical conditions that can impact AFM measurements, improvement in the resolution
229 of AFMs, and/or the precision of fitting force curves.

230 The relatively low variability in the values we measured for isolated sacculi from
231 *P. mirabilis* and *V. parahaemolyticus* cells (~16-25%) demonstrated a consistent reduction
232 in PG thickness for swarmer cells, suggesting that our measurements are sufficient for
233 comparing PG from vegetative and swarming cells, and demonstrating a connection
234 between PG and changes in cell mechanics. In contrast, the variability in AFM
235 measurements and analysis makes us less comfortable comparing absolute values of PG
236 thickness to those reported for bacteria in other papers.

237 To complement AFM measurements, we sought to measure the thickness of
238 native PG using electron cryotomography (ECT) on intact vegetative and swarmer cells
239 (Figs. 5C,D, S8, and S9). Although we were unable to resolve the thickness of native PG,
240 sub-tomogram-averaged ECT volumes of the *P. mirabilis* cell wall (Fig. 5C) indicated
241 that the distance between the inner and outer membrane of swarmer cells was smaller
242 than in vegetative cells (Figs. 5C,D). *P. mirabilis* vegetative cells had a characteristically
243 smooth membrane (Fig. S8A,B) that was similar to the presentation of the membrane
244 found along the lateral, cylindrical walls of swarmer cells (Fig. S8C,D). In contrast, the
245 polar regions of both *P. mirabilis* and *V. parahaemolyticus* swarmer cells had an
246 undulating outer membrane suggestive of an altered structure (Fig. S8E,F and S9D-F),
247 and *V. parahaemolyticus* cells had significant defects in their cell-envelope, including,
248 membrane budding, vesicle formation, and ruptured cell walls (Fig. S9D-F).

249
250 ***P. mirabilis* and *V. parahaemolyticus* swarmer cells are more sensitive to osmotic**
251 **stress than vegetative cells.** To complement cell stiffness measurements, we
252 investigated the mechanics of swarmer cells and filamented vegetative cells by
253 measuring their changes in length and volume in response to changes in osmotic
254 pressure, which will cause cells to shrink cells (in H₂O) and swell (in a NaCl solution)
255 (Fig. S10). We filamented *P. mirabilis*, *V. parahaemolyticus*, and control *E. coli* cells using
256 aztreonam to create a range of cell lengths that matched the lengths of *P. mirabilis* and *V.*

257 *parahaemolyticus* swarmer cells. We expected that low values of bending rigidity and
258 compositional and structural changes in PG would cause swarmer cells to elongate in
259 response to changes in osmotic pressure (in comparison to filamented, vegetative cells).
260 We found that *P. mirabilis* and *V. parahaemolyticus* swarmer cell extension in response to
261 osmotic shock was significantly larger than filamented, vegetative cells (Fig. 6). To
262 circumvent the cellular production of osmolytes to protect cells from large changes in
263 osmotic pressure during shock (typically produced within 1 min) (24), we used a
264 microfluidic device to rapidly switch between H₂O and a NaCl solution and measured
265 changes in cell length before cells adapted (Fig. S10).

266 Osmotic shifts produced small changes in the length (Fig. 6A) and width (Fig. 6B)
267 of vegetative filamented *P. mirabilis* cells compared to *E. coli* cells (Figs. 6A,B). In
268 contrast, *V. parahaemolyticus* vegetative cells substantially increased in cell length (Fig.
269 6C) compared to *E. coli* cells, with no observable change in cell width (Fig. 6D). In
270 response to osmotic upshifts (i.e., transitioning from H₂O to NaCl), *P. mirabilis* and *V.*
271 *parahaemolyticus* swarmer cells dramatically increased in cell length (Figs. 6A, C) (and to
272 a lesser extent, cell width for *P. mirabilis* but not for *V. parahaemolyticus*; Figs. 6B, D)
273 compared to vegetative cells. These results suggest that changes in *P. mirabilis* and *V.*
274 *parahaemolyticus* swarmer cell mechanics make them more responsive to osmotic
275 changes.

276

277 **Increased susceptibility of *P. mirabilis* and *V. parahaemolyticus* swimmers to the cell**
278 **wall-targeting antibiotics.** Although swarming colonies of bacteria display resistance to
279 many antibiotics (5), our experiments suggest *P. mirabilis* and *V. parahaemolyticus*
280 swimmers may have increased susceptibility to cell wall-targeting antibiotics that
281 further alter PG structure, composition, and properties. To determine the sensitivity of
282 *P. mirabilis* and *V. parahaemolyticus* swimmers to the cell wall-targeting antibiotics
283 cephalexin (inhibits PBP3 and 4) (25) and penicillin G (inhibits PBP3, 4, and 6), we
284 measured swimmer single-cell growth in the presence of the minimum inhibitory
285 concentration (MIC) of antibiotics in a microfluidic device (Figs. S11) for 3 h. The time
286 scale of this experiment was chosen based on two previous reports: 1) treating cells with
287 cephalexin for 3 h was sufficient to kill ~100% of a population of *E. coli* cells (26); and 2)
288 ~2 h of cephalexin treatment was sufficient to observe cell lysis of *E. coli* cells measured
289 by single cell growth (27).

290 Using a microfluidic device enabled us to supply cells with a source of
291 continuously replenished fresh growth media to ensure exponential cell growth and a
292 constant concentration of antibiotics. We found that the survival of *P. mirabilis* (66%)
293 and *V. parahaemolyticus* (64%) vegetative cells treated with 1X MIC of cephalexin was
294 slightly higher than *E. coli* cells (55%) (Figs. 7A, S12). Treating *P. mirabilis* and *V.*
295 *parahaemolyticus* swimmer cells with 1X MIC of cephalexin reduced survival to 37% and
296 19%, respectively (Figs. 7A, S12), indicating their increased susceptibility. Rates of cell

297 survival in the presence of penicillin G were similar to the use of cephalexin (Fig. 7A).
298 We characterized dead cells using microscopy to measure membrane blebbing, cell
299 lysis, and changes in the refractive index of cells.

300 Cell wall-targeting antibiotics are most effective against actively growing cells
301 (28, 29) and therefore increases in growth rate will reduce cell survival. To determine
302 whether a growth rate phenotype explains our observations, we normalized data for
303 cell length, and were unable to detect a change in the growth rate of swarmer cells
304 when they were treated with these two antibiotics (Fig. S13). We measured the mean
305 survival time of cells (the amount of time elapsed after treatment with drugs before cell
306 death) for *P. mirabilis* and *V. parahaemolyticus* swarmer cells treated with cephalixin and
307 penicillin G (Fig. 7B) and found that the survival time for these swarmer cells was lower
308 than that for vegetative cells (Fig. 7B), which is consistent with alterations in the PG.

309

310 **Discussion**

311 *P. mirabilis* is commonly associated with complicated urinary tract infections and
312 increased mortality in cases of bacteremia (30). Swarming is hypothesized to enable *P.*
313 *mirabilis* cell movement from the ureter to the kidney; in support of this hypothesis,
314 swarming deficient mutants have lower rates of host infection (31). We found that
315 during swarming, *P. mirabilis* and *V. parahaemolyticus* cells become more flexible due to
316 changes in PG composition and cell wall structure. Presumably this phenotype conveys

317 an adaptive advantage for cells that we hypothesize improves community motility by
318 enabling long swarmer cells to form cell-cell contacts that are demonstrated to enhance
319 motility. The adaptive advantage of swarming in *P. mirabilis* and *V. parahaemolyticus* is
320 offset by a decrease in their fitness, as cells become more sensitive to osmotic changes
321 and cell wall-targeting antibiotics, thereby creating an “Achilles heal” for targeting this
322 phenotype in infectious diseases. This study highlights the plasticity of bacteria (1), the
323 need for devising tests for treatments that measure efficacy against cells in a
324 physiological state relevant to specific infections, and re-considering the use of cell wall-
325 targeting antibiotics for treating UTIs in which *P. mirabilis* may be present.

326

327 **Materials and Methods**

328 **Bacterial strains and cell culture.** *P. mirabilis* strain HI4320, *V. parahaemolyticus* LM5674,
329 *Escherichia coli* MG1655 (CGSC #6300), and plasmids *pflhDC* (10) and *psula*(18) were
330 used for experiments used in this paper. *P. mirabilis* was grown in PLB nutrient medium
331 consisting of 1% peptone (weight/volume), 0.5% yeast extract (w/v), and 1% NaCl (w/v).
332 *V. parahaemolyticus* was grown in nutrient medium (HI medium) consisting of 2.5%
333 heart infusion (w/v) and 2.5% NaCl (w/v). *E. coli* was grown in lysogeny broth (LB)
334 consisting of 1% tryptone (w/v), 0.5% yeast extract (w/v), and 1% NaCl (w/v). All strains
335 were grown at 30 °C with shaking at 200 rpm. Additional data and methods are
336 described in Supplementary Information.

337 **Acknowledgements.** We thank Linda McCarter for *V. parahaemolyticus* LM5674,
338 Suckjoon Jun for the *psuA* plasmid, Cameron Scarlett and Molly Pellitteri-Hahn for
339 mass spectrometry support, and Julie Last for technical assistance with AFM
340 measurements. This research was supported by NIH grant 1DP2OD008735-01, National
341 Science Foundation grant DMR-1121288, a Mao Wisconsin Distinguished Graduate
342 Fellowship (to M.R.), and an NSF postdoctoral fellowship (#1202622 to P.M.O), and the
343 Howard Hughes Medical Institute.

344

345

346

347

348

349

350

351

352

353

354

355

356

357 References

- 358 1. Justice SS, Hunstad DA, Cegelski L, & Hultgren SJ (2008) Morphological
359 plasticity as a bacterial survival strategy. *Nat Rev Microbiol* 6(2):162-168.
- 360 2. Rajendram M, *et al.* (2015) Anionic phospholipids stabilize RecA filament
361 bundles in *Escherichia coli*. *Mol Cell* 60(3):374-384.
- 362 3. Copeland MF & Weibel DB (2009) Bacterial Swarming: A Model System for
363 Studying Dynamic Self-assembly. *Soft Matter* 5(6):1174-1187.
- 364 4. Kearns DB (2010) A field guide to bacterial swarming motility. *Nat Rev Microbiol*
365 8(9):634-644.
- 366 5. Butler MT, Wang Q, & Harshey RM (2010) Cell density and mobility protect
367 swarming bacteria against antibiotics. *Proc Natl Acad Sci U S A* 107(8):3776-3781.
- 368 6. Kim W, Killam T, Sood V, & Surette MG (2003) Swarm-cell differentiation in
369 *Salmonella enterica* serovar typhimurium results in elevated resistance to
370 multiple antibiotics. *J Bacteriol* 185(10):3111-3117.
- 371 7. Overhage J, Bains M, Brazas MD, & Hancock RE (2008) Swarming of
372 *Pseudomonas aeruginosa* is a complex adaptation leading to increased
373 production of virulence factors and antibiotic resistance. *J Bacteriol* 190(8):2671-
374 2679.
- 375 8. Lai S, Tremblay J, & Deziel E (2009) Swarming motility: a multicellular behaviour
376 conferring antimicrobial resistance. *Environ Microbiol* 11(1):126-136.
- 377 9. Hay NA, Tipper DJ, Gygi D, & Hughes C (1999) A novel membrane protein
378 influencing cell shape and multicellular swarming of *Proteus mirabilis*. *J Bacteriol*
379 181(7):2008-2016.
- 380 10. Tuson HH, Copeland MF, Carey S, Sacotte R, & Weibel DB (2013) Flagellum
381 density regulates *Proteus mirabilis* swarmer cell motility in viscous
382 environments. *J Bacteriol* 195(2):368-377.
- 383 11. Vollmer W & Seligman SJ (2010) Architecture of peptidoglycan: more data and
384 more models. *Trends Microbiol* 18(2):59-66.
- 385 12. Wang S, Arellano-Santoyo H, Combs PA, & Shaevitz JW (2010) Actin-like
386 cytoskeleton filaments contribute to cell mechanics in bacteria. *Proc Natl Acad Sci*
387 *U S A* 107(20):9182-9185.
- 388 13. Tuson HH, *et al.* (2012) Measuring the stiffness of bacterial cells from growth
389 rates in hydrogels of tunable elasticity. *Mol Microbiol* 84(5):874-891.
- 390 14. Wheeler R, *et al.* (2015) Bacterial Cell Enlargement Requires Control of Cell Wall
391 Stiffness Mediated by Peptidoglycan Hydrolases. *Mbio* 6(4):e00660.
- 392 15. Loskill P, *et al.* (2014) Reduction of the peptidoglycan crosslinking causes a
393 decrease in stiffness of the *Staphylococcus aureus* cell envelope. *Biophys J*
394 107(5):1082-1089.

- 395 16. Auer GK, *et al.* (2016) Mechanical Genomics Identifies Diverse Modulators of
396 Bacterial Cell Stiffness. *Cell Syst* 2(6):402-411.
- 397 17. Auer GK & Weibel DB (2017) Bacterial Cell Mechanics. *Biochemistry-U*s
398 56(29):3710-3724.
- 399 18. Amir A, Babaeipour F, McIntosh DB, Nelson DR, & Jun S (2014) Bending forces
400 plastically deform growing bacterial cell walls. *Proc Natl Acad Sci U S A*
401 111(16):5778-5783.
- 402 19. Gan L, Chen S, & Jensen GJ (2008) Molecular organization of Gram-negative
403 peptidoglycan. *Proc Natl Acad Sci U S A* 105(48):18953-18957.
- 404 20. Patrick JE & Kearns DB (2012) Swarming motility and the control of master
405 regulators of flagellar biosynthesis. *Mol Microbiol* 83(1):14-23.
- 406 21. Desmarais SM, *et al.* (2015) High-throughput, highly sensitive analyses of
407 bacterial morphogenesis using ultra performance liquid chromatography. *J Biol*
408 *Chem* 290(52):31090-31100.
- 409 22. Strating H, Vandenende C, & Clarke AJ (2012) Changes in peptidoglycan
410 structure and metabolism during differentiation of *Proteus mirabilis* into
411 swarmer cells. *Can J Microbiol* 58(10):1183-1194.
- 412 23. Yao X, Jericho M, Pink D, & Beveridge T (1999) Thickness and elasticity of gram-
413 negative murein sacculi measured by atomic force microscopy. *J Bacteriol*
414 181(22):6865-6875.
- 415 24. McLaggan D, Naprstek J, Buurman ET, & Epstein W (1994) Interdependence of
416 K⁺ and glutamate accumulation during osmotic adaptation of *Escherichia coli*. *J*
417 *Biol Chem* 269(3):1911-1917.
- 418 25. Eberhardt C, Kuerschner L, & Weiss DS (2003) Probing the catalytic activity of a
419 cell division-specific transpeptidase in vivo with beta-lactams. *J Bacteriol*
420 185(13):3726-3734.
- 421 26. Chung HS, *et al.* (2009) Rapid beta-lactam-induced lysis requires successful
422 assembly of the cell division machinery. *Proc Natl Acad Sci U S A* 106(51):21872-
423 21877.
- 424 27. Yao Z, Kahne D, & Kishony R (2012) Distinct single-cell morphological dynamics
425 under beta-lactam antibiotics. *Mol Cell* 48(5):705-712.
- 426 28. Tuomanen E, Cozens R, Tosch W, Zak O, & Tomasz A (1986) The Rate of Killing
427 of *Escherichia-Coli* by Beta-Lactam Antibiotics Is Strictly Proportional to the Rate
428 of Bacterial-Growth. *J Gen Microbiol* 132:1297-1304.
- 429 29. Spoering AL & Lewis K (2001) Biofilms and planktonic cells of *Pseudomonas*
430 *aeruginosa* have similar resistance to killing by antimicrobials. *J Bacteriol*
431 183(23):6746-6751.
- 432 30. Chen CY, *et al.* (2012) *Proteus mirabilis* urinary tract infection and bacteremia:
433 risk factors, clinical presentation, and outcomes. *J Microbiol Immunol Infect*
434 45(3):228-236.

435 31. Burall LS, *et al.* (2004) Proteus mirabilis genes that contribute to pathogenesis of
436 urinary tract infection: Identification of 25 signature-tagged mutants attenuated
437 at least 100-fold. *Infect Immun* 72(5):2922-2938.
438

439

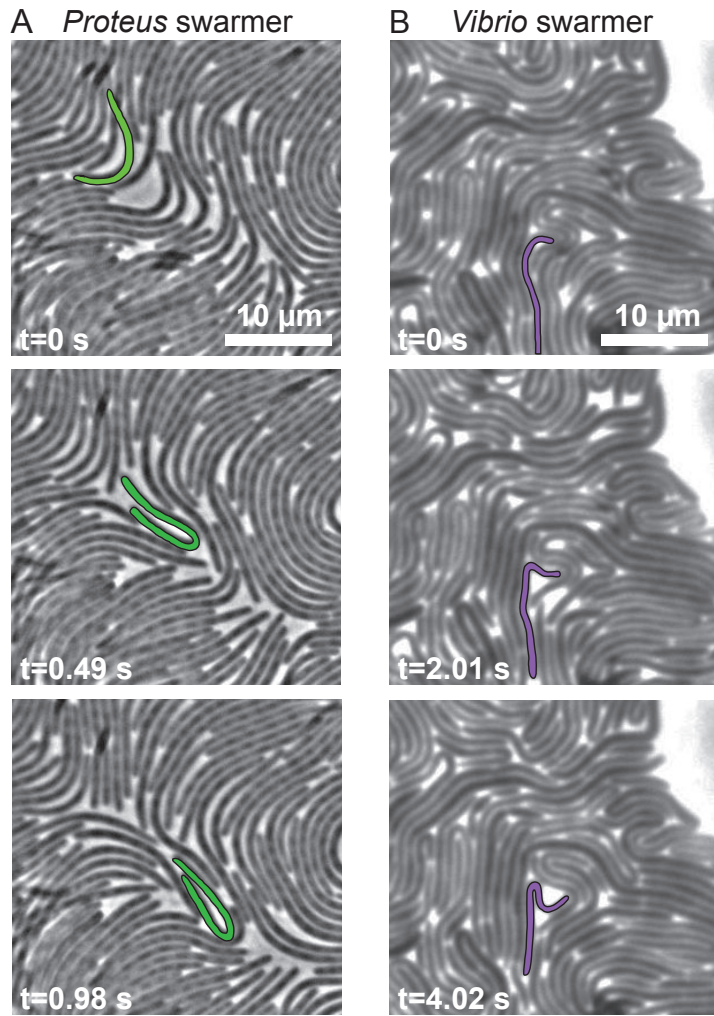
440

441

442 **FIGURES**

443 **Fig. 1.** Images demonstrating the flexibility of *P. mirabilis* and *V. parahaemolyticus*
444 swarmer cells. (A) Time-series of *P. mirabilis* swarmer cells in a colony actively moving
445 across the surface of a 1.5% agarose gel. A representative cell, false colored green, has a
446 generally straight shape at $t=0$ s and is bent in half at $t=0.98$ s. Most of the cells in this
447 frame are bending during this imaging sequence. (B) A time-series of *V. parahaemolyticus*
448 swarmer cells in a colony actively moving across the surface of a 1.4% agarose gel. A
449 representative cell (false colored purple) has a generally straight shape at $t=0$ s and is
450 bent in half at $t=4.02$ s.

451



452

453 Fig. 1

454

455

456

457

458

459

460

461 **Fig. 2.** Using a reloadable microfluidic-based assay to determine bacterial cell stiffness.

462 (A) Schematic of the microfluidic channel used to apply a user-defined shear force to

463 bend filamentous or swarmer cells. Single-sided green arrows depict the flow of fluid

464 through the central channel; the parabolic flow profile of the fluid is shown. Double-

465 sided green arrows indicate the vacuum chamber used to load cells into side channels

466 and to empty the device. (B) Cartoon of a flexible bacterium (left) and a stiff bacterium

467 (right) under flow force (V_{flow}). x_{max} indicates the deflection of cells in the flow; $2r$ = cell

468 diameter; L = cell length in contact with the flow force. (C) Representative images of

469 filamentous cells of *P. mirabilis* in no flow (left) and flow (right) conditions (top) and *P.*

470 *mirabilis* swarmers (bottom). Purple dashed lines indicate the position of a cell tip under

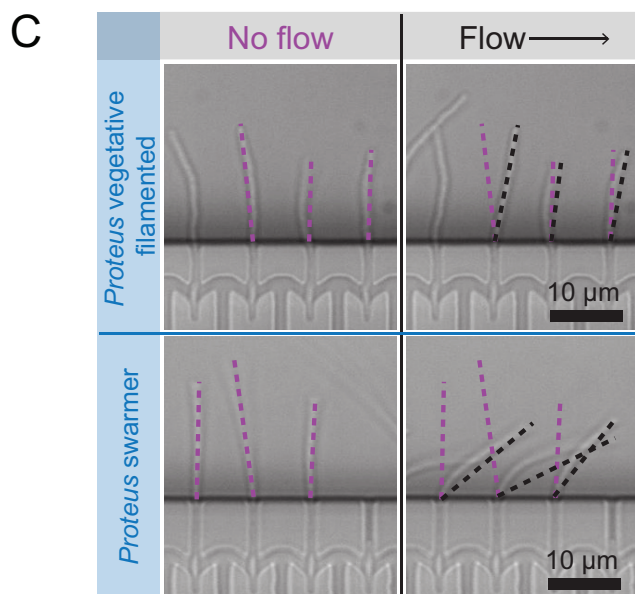
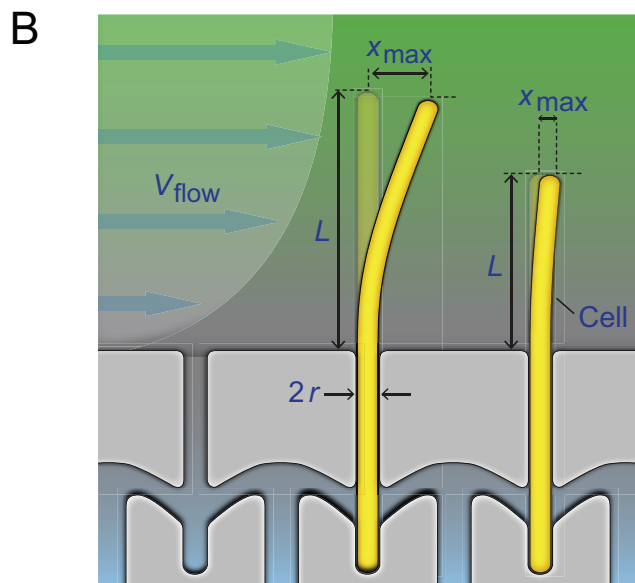
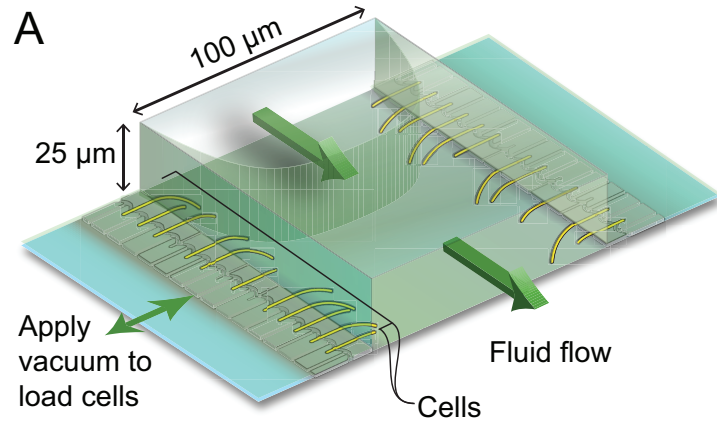
471 no flow conditions and black dashed lines illustrate the position after flow is applied

472 using a gravity-fed mechanism. The arrow indicates the direction of fluid flow in the

473 channel.

474

475



477 **Fig. 3.** *P. mirabilis* and *V. parahaemolyticus* swarmer cells have a lower bending rigidity
478 than vegetative cells. We measured the bending rigidity of *P. mirabilis* and *V.*
479 *parahaemolyticus* swarmer cells and filamentous vegetative cells in a microfluidic flow
480 assay and included measurements of vegetative *E. coli* cells. *P. mirabilis* swarmers
481 exhibited 15-fold lower bending rigidity than vegetative cells; *V. parahaemolyticus*
482 swarmers were 3-fold less rigid than vegetative cells. Overexpression of FlhDC (from
483 the plasmid-encoded *pflhDC*) had little effect on the stiffness of *P. mirabilis* vegetative
484 and swarmer cells. Error bars represent the 95% confidence interval of a fit to data. $n >$
485 100 cells, from at least 3 independent experiments.

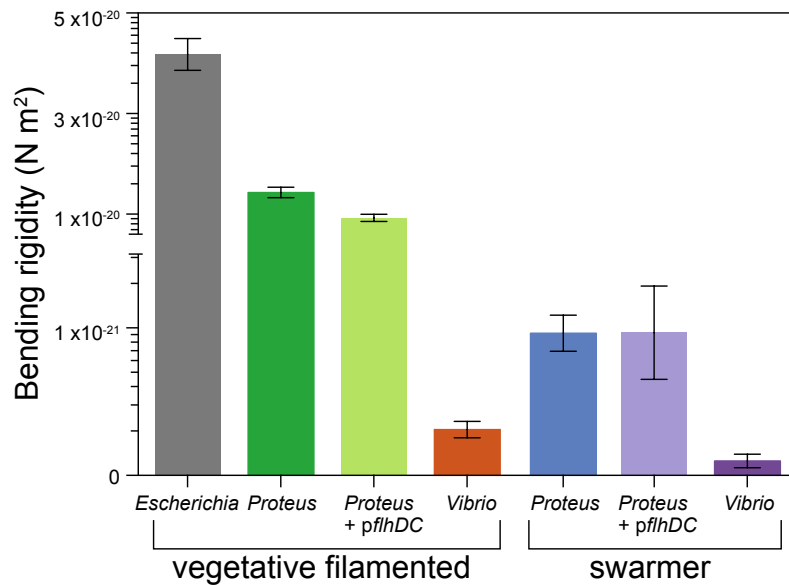
486

487

488

489

490



491

492 **Fig 3.**

493

494

495

496

497

498

499

500

501

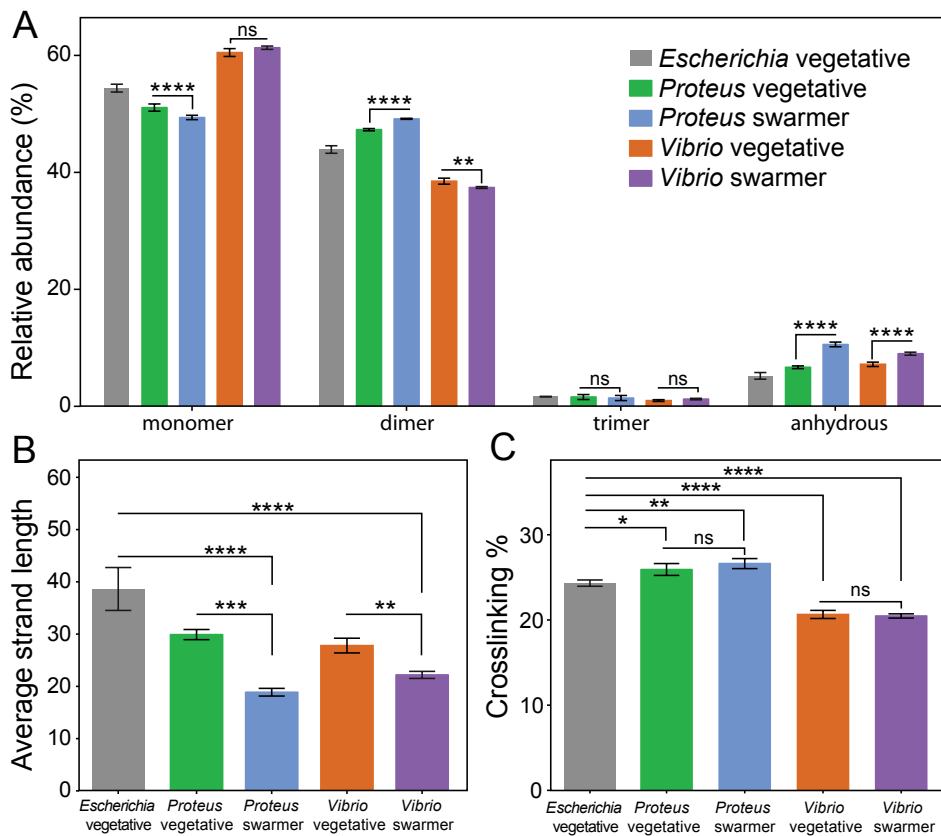
502

503

504 **Fig. 4.** Alterations in the PG muropeptide composition of *P. mirabilis* and *V.*
505 *parahaemolyticus* swarmer cells. (A) UPLC-MS data reveal that the muropeptide
506 composition of *P. mirabilis* and *V. parahaemolyticus* vegetative and swarmer cells differs
507 slightly in the abundance of monomer, dimer, and anhydrous-terminated saccharides.
508 (B) We observed a relative increase in the amount of anhydrous-containing saccharides
509 in swarmers consistent with a decrease in polysaccharide strand length. (C) There was
510 no change in PG cross-linking of *P. mirabilis* and *V. parahaemolyticus* vegetative and
511 swarmer cells, although *V. parahaemolyticus* does display a lower level of cross-linking. *n*
512 = 3 biological replicates. Error bars represent the standard deviation of the mean.
513 For (A-C), significance was determined via two-way analysis of variance: * $P \leq 0.05$, ** $P \leq$
514 0.01 , *** $P \leq 0.001$, **** $P \leq 0.0001$, ns = not significant ($P > 0.05$).

515

516



517

518 **Fig 4.**

519

520

521

522

523

524

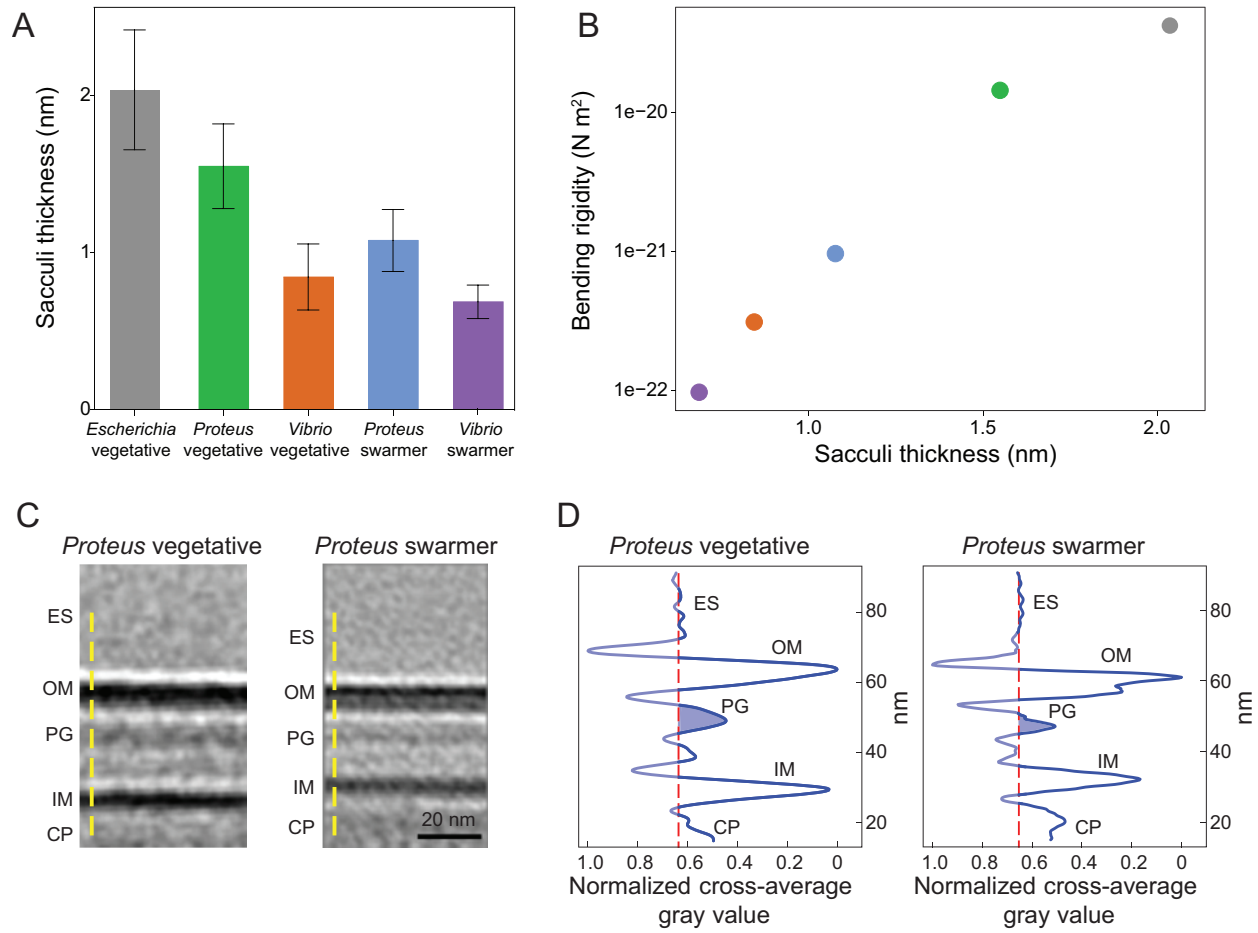
525

526

527 **Fig. 5.** AFM reveals the PG layer of *P. mirabilis* and *V. parahaemolyticus* swarmer cells is
528 thinner than in vegetative cells and ECT demonstrates a reduced membrane-to-
529 membrane distance. (A) Sacculi were isolated from cells, dried, and imaged by AFM.
530 The thickness of swarmer cell PG was reduced compared to vegetative cells. We
531 analyzed >65 vegetative cells of *E. coli*, *P. mirabilis*, and *V. parahaemolyticus*, >65 *P.*
532 *mirabilis* swarmer cells, and 7 *V. parahaemolyticus* swarmer cells. Error bars represent the
533 standard deviation of the mean. (B) Bending rigidity and cell wall thickness display an
534 approximately exponential relationship ($R^2=0.9874$). (C) Sub-tomogram-averaged ECT
535 volume images of the *P. mirabilis* vegetative (left) and swarmer (right) cell wall. Two
536 central slices of sub-tomogram average volume images with normalized image densities
537 are shown. Yellow dashed line indicates the orientation used for gray-value
538 measurements. ES, extracellular space; OM, outer membrane; PG, peptidoglycan; IM,
539 inner membrane; CP, cytoplasm. (D) The density profile of sub-tomogram-averaged
540 ECT volume images reveals a reduced membrane-to-membrane distance in swarmer
541 cells. The vertical axis is the normalized gray value with the darkest value equal to 0
542 and the lightest value equal to 1. The red dashed line denotes the average gray value of
543 the extracellular space and serves as a reference for the background; the blue shaded
544 area indicates the thickness of the putative PG layer.

545

546



547

548 **Fig 5.**

549

550

551

552

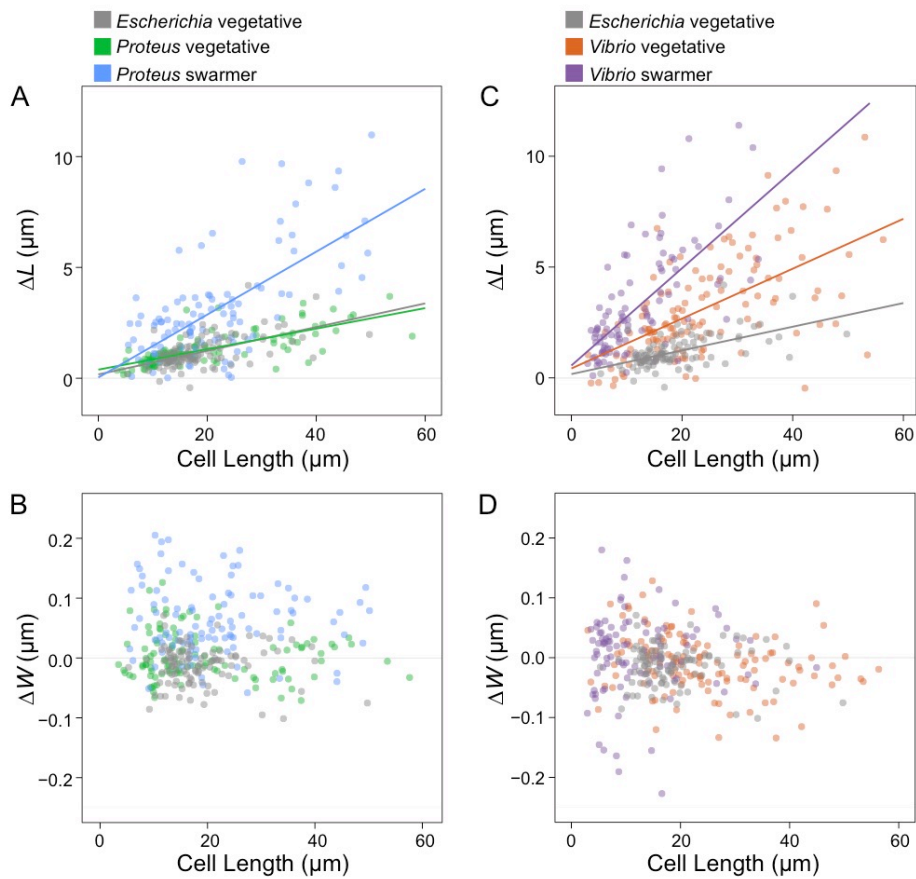
553

554

555

556

557 **Fig. 6.** Swarmer cells increase in cell extension during osmotic shock. We calculated ΔL
558 as (cell length in water – cell length in 1 M NaCl) and performed a similar calculation
559 for ΔW , substituting cell width. Cell length indicates length prior to osmotic shock. We
560 filamented all vegetative cells using aztreonam to grow them to lengths that were
561 comparable with *P. mirabilis* and *V. parahaemolyticus* swarmers. Lines indicate linear fits
562 to single-cell measurements (circles) of $n > 100$ cells from at least 3 independent
563 experiments. (A) *P. mirabilis* swarmer cells have an increase in extension (ΔL) under
564 osmotic shock compared to *E. coli* and *P. mirabilis* vegetative cells. (B) *V. parahaemolyticus*
565 vegetative and swarmer cells have an increase in extension (ΔL) under osmotic shock
566 compared to *E. coli*. (C) *P. mirabilis* swarmer cells have an increase in ΔW compared to *E.*
567 *coli*; *P. mirabilis* vegetative cells display a slight decrease in width and increased cell
568 length. (D) There was no observable change in ΔW of *V. parahaemolyticus* swarmer and
569 vegetative cells.
570



571

572 **Fig 6.**

573

574

575

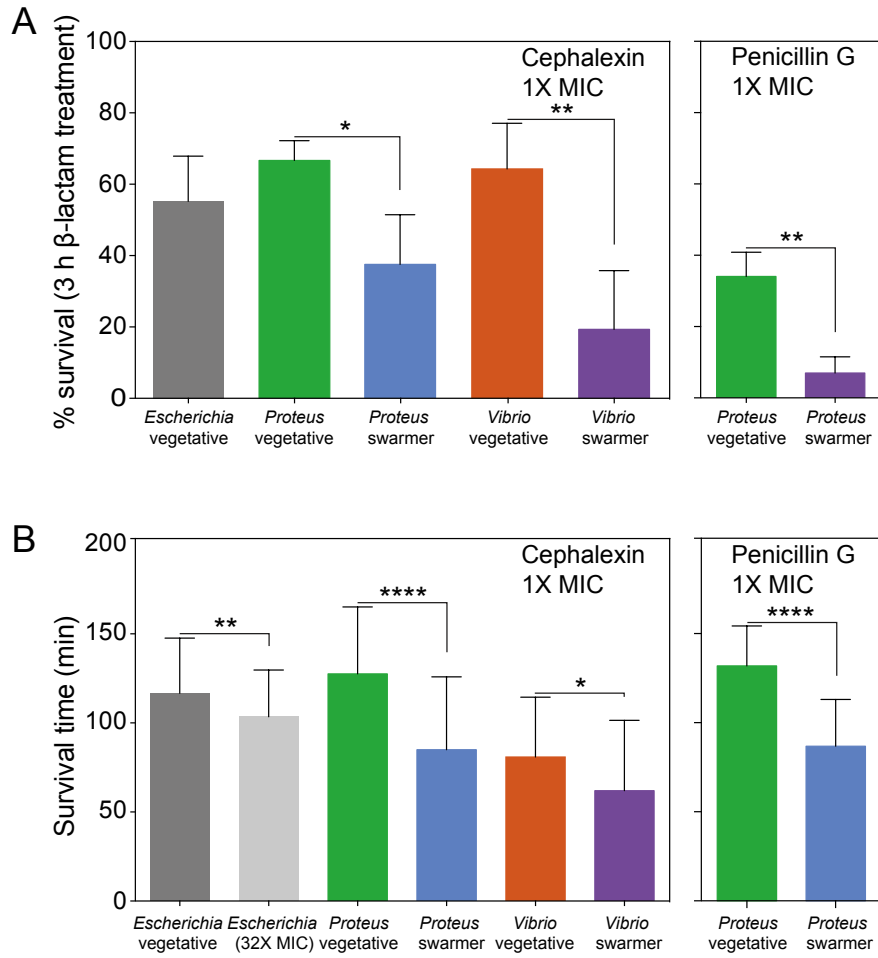
576

577

578

579

580 **Fig. 7.** Swarmer cells are more susceptible to antibiotics that target the cell wall than are
581 vegetative cells. (A) Survival of cells treated with 1X MIC of cephalexin after 3 h of
582 incubation. We define percent survival as $(\text{cell count}_{\text{no lysis}} / \text{cell count}_{\text{total}}) \times 100$. *P.*
583 *mirabilis* and *V. parahaemolyticus* swarmer cells exhibit decreased levels (~30%) of
584 survival compared to vegetative cells; $n \geq 90$ cells from at least two independent
585 experiments. A similar decrease occurred when *P. mirabilis* was treated with penicillin
586 G; $n \geq 77$ cells from at least two independent experiments). Error bars represent the
587 standard deviation of the mean. (B) After exposure to cephalexin or penicillin G, the
588 survival time of *P. mirabilis* and *V. parahaemolyticus* swarmers was 2~3 fold lower than
589 for vegetative cells. Survival time was determined for ≥ 49 cells that lysed from at least 2
590 independent experiments. Significance in A-B was determined two-tailed t-test: * $P \leq$
591 0.05, ** $P \leq 0.01$, **** $P \leq 0.0001$.
592



593

594 Fig 7.